

Measurement of the ultrafast lighthouse effect using a complete spatiotemporal pulse-characterization technique

ZHE GUANG,* MICHELLE RHODES, AND RICK TREBINO

School of Physics, Georgia Institute of Technology, 837 State Street, Atlanta, Georgia 30332, USA

*Corresponding author: zguang3@gatech.edu

Received 12 May 2016; revised 27 July 2016; accepted 28 July 2016; posted 4 August 2016 (Doc. ID 265087); published 24 August 2016

Three of the four spatiotemporal pulse amplitude couplings—spatial chirp, angular dispersion, and pulse-front tilt—are well known for their important roles in optics and, especially, in ultrafast optics. The remaining one, only recently identified, corresponds to the pulse arrival time variation with angle and is known as the “ultrafast lighthouse effect.” This effect has important applications in attosecond science, but its characterization has not yet received much attention. In this work, we generate an ultrafast lighthouse and measure it using a recently developed single-frame complete spatiotemporal pulse-characterization technique called STRIPED FISH. We discuss in great detail the measured couplings in different domains and their roles in generating the ultrafast lighthouse effect. In addition, we display the propagation of the measured ultrafast lighthouse with an intuitive movie plot over space and time. We conclude that STRIPED FISH provides a simple and informative approach for measuring the ultrafast lighthouse effect and also other possible spatiotemporal distortions in the pulse, in both the horizontal and vertical dimensions. © 2016 Optical Society of America

OCIS codes: (320.0320) Ultrafast optics; (320.7100) Ultrafast measurements.

<http://dx.doi.org/10.1364/JOSAB.33.001955>

1. INTRODUCTION

Although known for centuries, spatiotemporal field couplings have recently taken on more important roles, especially in ultrafast optical applications such as pulse shaping [1], spatiotemporal waveform manipulation [2], and simultaneous spatial and temporal focusing for microscopy [3], to name a few. At the same time, undesirable pulse field couplings (in this case, usually referred to as “distortions”) can arise from misalignment [4], optical aberrations [5], or strong laser–matter interactions [6,7]. They can cause difficulties such as a reduced intensity at the focus, undesired satellite pulses in amplification systems, and so on. All these situations call for better understanding and measurement of the pulse-coupling effects.

There has been significant recent progress in understanding the coupling effects and their relations to each other, which once were not very intuitive. For example, pulse-front tilt, a commonly observed pulse coupling in space and time, is usually generated using angularly dispersive elements such as prisms, gratings, and etalons [8–10]. The general relation between pulse-front tilt and angular dispersion was not clear until an argument based on the Fourier transform shift theorem arose to explain their effective equivalence [9]. However, it was then noticed that pulse-front tilt can also occur in the

complete absence of angular dispersion, simply from the simultaneous presence of temporal chirp and spatial chirp (the previous argument had implicitly neglected spatial chirp) [11]. This unexpected complexity hinted at the complex relationships among different couplings and highlighted why they remained poorly understood and investigated over the years.

Recently, our group had developed a mathematically simple yet complete approach to describe the first-order spatiotemporal couplings in the pulse [12,13]. Because various domains (time and frequency as well as space and spatial frequency) are Fourier-transform conjugates, any pulse-field expression in one domain [e.g., the spatiotemporal (x, t) domain] can be transformed into any other domain [e.g., the spatial-frequency-spectral (k, ω) domain] by performing one or two Fourier transforms with respect to space and/or time. In the theory of first-order spatiotemporal couplings, the pulse field is approximated by a Gaussian expression over space and time, with the cross term in the exponent representing coupling in one domain. For example, the pulse field in the spatiotemporal (x, t) domain is

$$E(x, t) \propto \exp(\tilde{Q}_{xx}x^2 + 2\tilde{Q}_{xt}xt - \tilde{Q}_{tt}t^2), \quad (1)$$

where we have ignored the y dependence of the transverse electric field $E(x, y, t)$ for simplicity in our discussion. In the exponent

Table 1. Gaussian Pulse Field Expressions with First-Order Spatiotemporal Couplings^a

| Domain | Expression | Real Part | Amplitude Coupling | Imaginary Part | Phase Coupling |
|---------------|---|-------------------------------|-----------------------------|-------------------------------|----------------------------|
| (x, t) | $E(x, t) \propto \exp(\tilde{Q}_{xx}x^2 + 2\tilde{Q}_{xt}xt - \tilde{Q}_{tt}t^2)$ | $\text{Re}\{\tilde{Q}_{xt}\}$ | Pulse-front tilt | $\text{Im}\{\tilde{Q}_{xt}\}$ | Wave-front rotation |
| (x, ω) | $E(x, \omega) \propto \exp\{R_{xx}x^2 + 2R_{x\omega}x\omega - R_{\omega\omega}\omega^2\}$ | $\text{Re}\{R_{x\omega}\}$ | Spatial chirp | $\text{Im}\{R_{x\omega}\}$ | Wave-front tilt dispersion |
| (k, t) | $E(k, t) \propto \exp(P_{kk}k^2 + 2P_{kt}kt - P_{tt}t^2)$ | $\text{Re}\{P_{kt}\}$ | Ultrafast lighthouse effect | $\text{Im}\{P_{kt}\}$ | Angular temporal chirp |
| (k, ω) | $E(k, \omega) \propto \exp\{S_{kk}k^2 + 2S_{k\omega}k\omega - S_{\omega\omega}\omega^2\}$ | $\text{Re}\{S_{k\omega}\}$ | Angular dispersion | $\text{Im}\{S_{k\omega}\}$ | Angular frequency chirp |

^aIn each spatiotemporally coupled domain, a pair of amplitude and phase distortions is defined corresponding to the real and imaginary parts of the cross term, respectively. The ultrafast lighthouse effect is the amplitude-coupling term in the spatial-frequency-temporal (k, t) domain. Their relations are discussed in Ref. [12].

of Eq. (1), the real and imaginary parts of the cross term \tilde{Q}_{xt} correspond to the amplitude and phase couplings in the spatiotemporal (x, t) domain, respectively. Specifically, the real part $\text{Re}\{\tilde{Q}_{xt}\}$ corresponds to the pulse-front tilt and the imaginary part $\text{Im}\{\tilde{Q}_{xt}\}$ describes the phase variation coupled over x and t , indicating the wave-front direction change with respect to time, hence the term “wave-front rotation.”

Because Gaussian expressions always Fourier transform to Gaussians, analogous expressions to Eq. (1) naturally occur in all three other spatiotemporally coupled domains, (x, ω) , (k, t) , and (k, ω) . Similarly, in each of these domains, a pair of amplitude and phase couplings can be defined. The field expressions, cross terms, and corresponding pulse-coupling effects in each domain are summarized in Table 1.

In addition to explaining two different sources of the pulse-front tilt, this theoretical framework also provides insight into an interesting pulse amplitude coupling effect in the spatial-frequency-temporal (k, t) domain, termed the “ultrafast lighthouse effect” [12]. The ultrafast lighthouse effect is a pulse amplitude effect that relates the spatial-frequency domain to the time domain. It describes the pulse amplitude propagation direction change as a function of time (also known as “time versus angle”) [14]. In analytical field expressions, this effect comes in a form of real coefficient before the product of spatial frequency k and time t in the exponential. The name “lighthouse” follows from an analogy between the ultrashort pulse propagation with such coupling and the light emanated from a lighthouse—with different propagation directions at different time, generating a light pattern spiraling out from the center.

The four pulse spatiotemporal amplitude couplings are important in many aspects. As in Table 1, these four couplings are pulse-front tilt, spatial chirp, angular dispersion, and ultrafast lighthouse effect. Each of the four effects occurs in one particular domain, representing the pulse energy distribution in that domain, and their relations are described by Fourier transforms [12].

In contrast to the other three spatiotemporal amplitude couplings, the ultrafast lighthouse effect has not been thoroughly investigated. Many common and very useful applications have been found for the other three amplitude couplings in optics and especially ultrafast optics. For example, spatial chirp in the spatio-spectral (x, ω) domain and angular dispersion in the spatial-frequency-spectral (k, ω) domain have been used to spatially separate frequencies since Newton’s time and are now in common use for pulse compressors [15] and pulse shapers [16]. Pulse-front tilt, in the spatiotemporal (x, t) domain, has been used for laser material processing [17,18] and ultrashort

pulse measurement [19–21]. These three well-known spatiotemporal distortions are also relatively readily characterized [22]. Perhaps as a result of its lagging behind the study of other couplings, important applications have recently been found for the ultrafast lighthouse effect, particularly in attosecond science. By manipulating couplings in an intense few-cycle incident pulse that interacts with a plasma mirror or gas medium [23–29], the lighthouse effect can generate a high-harmonic attosecond pulse train containing pulses, each diverging at a different angle. It is important to note that the attosecond lighthouse is composed of a train of pulses while the ultrafast lighthouse effect is usually concerned about one single pulse which can be of any possible duration. In the far field, if the right conditions are fulfilled [27], the attosecond pulses can then be spatially separated from each other to yield isolated attosecond pulses that are convenient for use in pump-probe experiments and photonic streaking applications [24]. On the other hand, like all other distortions, if the ultrafast lighthouse effect occurs unknowingly or is left uncharacterized, it can have undesirable effects such as causing damage to facilities, distortion of experimental results, and misleading data interpretations. Considering the unique properties of the ultrafast lighthouse effect and the fact that there has been no device shown for its complete measurement, we propose here a compact method for its characterization, and demonstrate our results from measurement to better understand this coupling effect.

We should also mention that the ultrafast lighthouse effect and all other first-order spatiotemporal couplings actually represent only a tiny fraction of all possible couplings or distortions in the pulse, and pulses do not always possess Gaussian profiles. Therefore, a technique that can provide the complete spatiotemporal field information would be useful and beneficial in many pulse-measurement tasks.

2. MEASURING SPATIOTEMPORAL COUPLINGS WITH STRIPED FISH

In presence of pulse-field spatiotemporal couplings, any measurement that separately characterizes the pulse spatial profile and pulse temporal profile (by averaging over the other) would be doomed to fail. It is therefore important to measure all the details of the spatiotemporal field $E(x, y, t)$ completely, and we will do this for the ultrafast lighthouse effect.

We recently developed a single-frame complete spatiotemporal field measurement technique called spatially and temporally resolved intensity and phase evaluation device: full

information from a single hologram (STRIPED FISH) [30,31]. In operation, it involves splitting off part of the beam, which then gets spatially filtered and temporally measured by frequency-resolved optical gating (FROG) [32,33]. This yields a spatiotemporally simple reference pulse, that is, a pulse with a known smooth spatial profile and a known temporal profile, essentially free of spatiotemporal couplings. This reference pulse is then used to measure the potentially spatiotemporally complex unknown pulse. These two beams are made to cross at a small angle vertically at the entrance of STRIPED FISH device, which is composed of a two-dimensional coarse grating [also called a diffractive-optical element (DOE)], an interference bandpass filter (IBPF), two imaging lenses, an apodizing neutral density filter (ANDF), and a camera [31]. The DOE and IBPF generate a slightly rotated array of quasi-monochromatic beams, each at a different frequency, which finally form many holograms on one camera frame simultaneously. With knowledge of the reference pulse, holograms at different frequencies can yield the unknown pulse spatial field $E(x, y, \omega)$ at multiple frequencies. Then the complete spatiotemporal field $E(x, y, t)$ can be obtained by performing an inverse Fourier transform of $E(x, y, \omega)$. The recorded camera frame, also called the “STRIPED FISH trace” [34], is itself informative and offers an immediate insight about the unknown pulse structure.

Because STRIPED FISH retrieves the unknown pulse spatial field at multiple frequencies, it operates in the spatio-spectral (x, ω) domain. Fourier transforming the spatiotemporal (x, t) domain expression Eq. (1) with respect to time t yields the Gaussian field expression in the spatio-spectral (x, ω) domain:

$$E(x, \omega) \propto \exp\{R_{xx}x^2 + 2R_{x\omega}x\omega - R_{\omega\omega}\omega^2\}. \quad (2)$$

In this domain, as shown in Table 1, the amplitude-coupling term $\text{Re}\{R_{x\omega}\}$ represents the spatial chirp and the phase-coupling term $\text{Im}\{R_{x\omega}\}$ represents the wave-front tilt dispersion, which describes the wave-front direction change with respect to frequency. Both the spatial chirp and wave-front tilt dispersion can be observed directly from STRIPED FISH traces [34].

It is also worth noting that since all first-order spatiotemporal couplings are related by Fourier transforms, any coupling in one particular domain would generally mean the existence of couplings in other domains except for a few coincidental cases [12]. Given the measured field value in the spatio-spectral (x, ω) domain, one can perform a Fourier transform or two to yield the field values and couplings in all other domains.

3. GENERATION AND MEASUREMENT OF THE ULTRAFAST LIGHTHOUSE EFFECT

The ultrafast lighthouse effect lives in the spatial-frequency-temporal (k, t) domain, so we Fourier transform Eq. (1) with respect to the spatial coordinate x to obtain

$$E(k, t) \propto \exp(P_{kk}k^2 + 2P_{kt}kt - P_{tt}t^2). \quad (3)$$

As shown in Table 1, the amplitude coupling $\text{Re}\{P_{kt}\}$ is the ultrafast lighthouse effect and the phase term $\text{Im}\{P_{kt}\}$ is the angular temporal chirp, which we mention here for completeness but is outside the scope of this paper.

There is no single optic that can directly generate ultrafast lighthouse effect (unlike, say, a prism for angular dispersion). However, because the couplings are all interrelated, one can induce the lighthouse effect by manipulating other couplings equivalently. Specifically, from the Gaussian field expressions in the spatiotemporal (x, t) domain [Eq. (1)] and the spatial-frequency-temporal (k, t) domain [Eq. (3)], one can derive a relation between the coupling coefficients:

$$P_{kt} = \frac{i \tilde{Q}_{xt}}{2 \tilde{Q}_{xx}}. \quad (4)$$

In terms of real and imaginary parts, the ultrafast lighthouse effect corresponds to

$$\text{Re}\{P_{kt}\} = \frac{1}{2} \frac{-\text{Im}\{\tilde{Q}_{xt}\}\text{Re}\{\tilde{Q}_{xx}\} + \text{Re}\{\tilde{Q}_{xt}\}\text{Im}\{\tilde{Q}_{xx}\}}{|\tilde{Q}_{xx}|^2}. \quad (5)$$

In this context, we have identified $\text{Re}\{\tilde{Q}_{xt}\}$ as the pulse-front tilt and $\text{Im}\{\tilde{Q}_{xt}\}$ as the wave-front rotation. The \tilde{Q}_{xx} term is straightforward to understand: its real part defines the beam size and its imaginary part is the wave-front curvature [12]. So Eq. (5), for the ultrafast lighthouse effect or time vs. angle, can be written in terms of pulse-front tilt, wave-front curvature, and wave-front rotation as

$$\text{TVA} = -2\text{WFR} + 2\text{PFT} \times \text{WFC}. \quad (6)$$

This expression implies that the ultrafast lighthouse effect can result from either wave-front rotation or the combination of pulse-front tilt and focusing. Wave-front rotation, as a phase-coupling effect in the spatiotemporal (x, t) domain, can be induced by spatial chirp to form lighthouses [23]. Alternatively, the lighthouse effect can be generated by having both pulse-front tilt, which is an amplitude coupling easily obtainable from gratings or prisms (through angular dispersion or simultaneous temporal and spatial chirp), and wave-front curvature, which can be easily introduced by a focusing lens or curved mirror. Here we take advantage of the latter approach, generating the ultrafast lighthouse effect by focusing a pulse with pulse-front tilt.

An excellent interpretation of how a focusing pulse-front tilt can generate ultrafast lighthouse effect appears in Ref. [35], and we adopt it here to suit our case. As in Fig. 1(a), a pulse with pulse-front tilt is incident onto a focusing lens. Due to the pulse-front tilt, the uppermost part in the pulse arrives first at time $t_0 - \delta$ and the lowermost part arrives last at time $t_0 + \delta$, with t_0 being the pulse central arrival time. Because the focusing lens maps incident beam position to propagation angle around its focus, the uppermost part (with earliest arrival time) will propagate at a downward angle and the lowermost part (with latest arrival time) will propagate upward. For regions of the beam in between, the propagation angles are closer to the optical axis and the arrival time is intermediate between the two extreme cases. Therefore, around the lens focus, the pulse will propagate at different angles at different arrival times, hence the ultrafast lighthouse effect.

To measure the ultrafast lighthouse effect, we built an apparatus as sketched in Fig. 1(b). The output pulse from a Ti:sapphire oscillator, centered at 800 nm wavelength and with a 25 nm FWHM spectral bandwidth, was temporally chirped and sent through a spatial filter comprising two focusing lenses

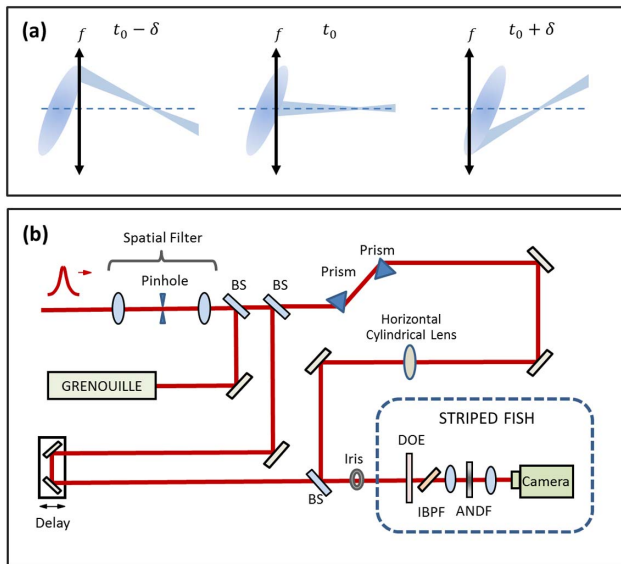


Fig. 1. (a) Generating the ultrafast lighthouse effect by focusing a pulse with pulse-front tilt, as discussed in Ref. [35] (Fig. 2). The pulse-front tilt is introduced to the pulse by a prism pair, and a focusing lens maps the incident beam position to propagation angle around its focus, generating the ultrafast lighthouse effect. (b) Apparatus for measuring the ultrafast lighthouse effect using STRIPED FISH (device shown in dashed blue outline). Pulses from a Ti:sapphire laser passed through a spatial filter and were characterized by a FROG device (GRENOUILLE). In one arm, the Mach-Zehnder interferometer contained the reference pulse and a delay stage for synchronization and, in the other arm, it contained a prism pair to introduce pulse-front tilt and a cylindrical lens to horizontally focus so as to generate the ultrafast lighthouse effect. The reference pulse and unknown pulse to be measured were finally combined into the STRIPED FISH device, composed of the DOE, IBPF, ANDF, imaging lenses, and a camera.

(with 100 mm and 200 mm focal lengths) and one pinhole (75 μm). Using a beam splitter (BS), part of the pulse energy was sent to a FROG device (Swamp Optics, GRENOUILLE model 8-20 USB) [36]. Most of the energy ($\sim 90\%$) propagated through the first BS to a second BS, the reflected beam from which served as the reference pulse, which was delayed by a translation stage to synchronize with the transmitted pulse in the other arm. The transmitted pulse from the first BS passed through a prism pair, which introduced spatial chirp to the pulse, together with its temporal chirp yielding the pulse-front tilt [11]. Next, the pulse-front tilted pulse was horizontally focused by a 150 mm cylindrical lens. Finally, the two beams were combined by a third BS into the STRIPED FISH device.

4. INTERPRETATION OF THE EXPERIMENTAL RESULTS

The measured STRIPED FISH trace and electric field retrieved from it contain a wealth of information. We first analyze the measured trace for signatures of the spatiotemporal couplings in the (x, ω) domain. Then, from the retrieved spatio-spectral field $E(x, y, \omega)$, we discuss the amplitude and phase variations over space and frequency. We then confirm the presence of ultrafast

lighthouse effect by showing that different spatial regions of the pulse have different propagation directions and arrival times. Finally, we display the lighthouse propagation using a movie plot over space and time, in which the z -dependence of the pulse was determined by computing diffraction integrals of the measured transverse complex field $E(x, y, t)$. As the pulse propagation movie is the final output file that displays all the measured information, readers may as well skim the analysis below (if not very interested in the details) to directly view the final results in Fig. 6 of this paper.

Figure 2(a) shows the STRIPED FISH trace, made of a 5×7 array of holograms. These holograms were created from interference of the reference pulse and the unknown pulse. By using the ANDF in STRIPED FISH, we obtained approximately uniformly distributed intensities among the holograms [31]. The effect of the ANDF was calibrated to determine the relative intensities of the various spectral components of the unknown pulse. In the trace, central wavelengths (or frequencies) of the holograms increased (or decreased) from the left side to right because the transmitted wavelengths of the IBPF depend on the horizontal incidence angles of the diffracted beams, and the horizontal incident angles were mapped onto different horizontal positions on the camera. Also, apparently each hologram contained curved fringes, which showed the wave-front curvature, and the fringes varied slightly from hologram to hologram, which indicated the difference in spatial phase at different frequencies. Additionally, when we examined the overall holographic pattern, we discovered that the holograms showed a slight horizontal shift from left to right, from small to large wavelengths, with respect to their centers. These differences in

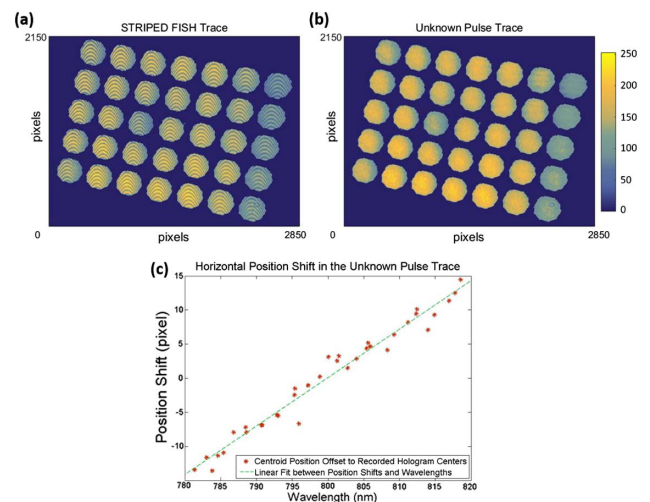


Fig. 2. Measured STRIPED FISH trace analysis. (a) STRIPED FISH trace from the interference of unknown and reference pulses. The trace shows approximately uniformly distributed intensities from order to order. A total of 35 holograms were used for unknown pulse retrieval, with increasing wavelengths from left to right in the trace. (b) The unknown pulse spatio-spectral profile, recorded by blocking the reference arm. The trace contains 35 diffractive orders with spatial intensities shifting with wavelengths in the horizontal direction. (c) The intensity-weighted centroid shift is plotted over wavelength and a linear fit is shown by a green line, which directly indicates the presence of spatial chirp in the unknown pulse.

fringe structure and hologram position shift indicated that spatial chirp and wave-front tilt dispersion, as the amplitude and phase couplings in the spatio-spectral (x, ω) domain, existed in the unknown pulse [34].

To more clearly demonstrate the position shift, we blocked the reference arm and recorded the unknown pulse alone with STRIPED FISH. Instead of recording holograms on the trace, we obtained on the camera spots representing the spectrally resolved spatial profile of the unknown pulse, as shown in Fig. 2(b). To quantitatively demonstrate this, in Fig. 2(c), we plot the intensity-weighted centroid offset from the recorded centers of the holograms for all 35 diffractive orders over their filtered wavelengths. Along the horizontal direction, centroids of these 35 diffractive orders shifted from left (minus) to right (positive) with increasing wavelengths, forming an almost linear dependence on wavelengths as shown by the green dashed line. Spatial profiles at small and large wavelengths were shifted farthest away from the center, confirming the presence of spatial chirp.

Phase couplings, such as wave-front tilt dispersion, are more indirect to observe. As a result, we must first retrieve the complete unknown pulse field $E(x, y, \omega)$ from the holograms. From each recorded hologram, the unknown pulse spatial information for one particular frequency $E(x, y, \omega_0)$ was retrieved. For example, in Fig. 3(a), we show the retrieved spatial phase at 800.05 nm using the hologram located at the center of

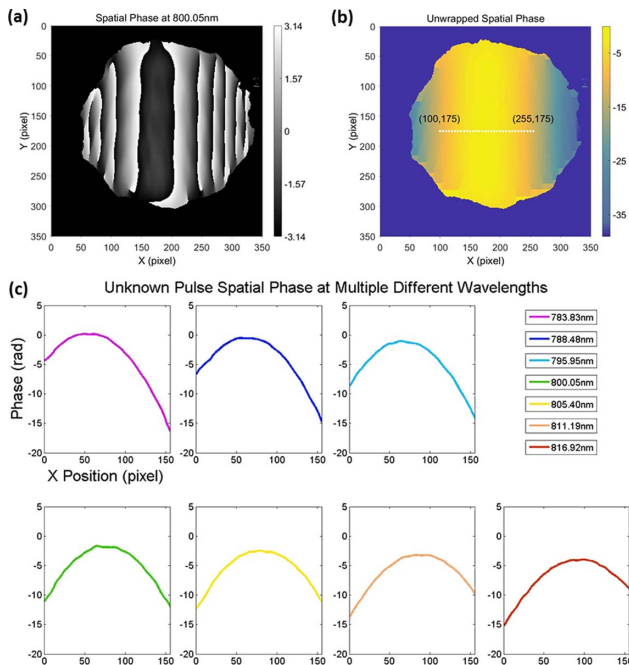


Fig. 3. Spatial phase measured by STRIPED FISH. (a) Spatial phase plot for 800.05 nm, retrieved from the central hologram in Fig. 2(a). (b) A two-dimensional phase-unwrapping algorithm unwrapped the phase over x and y to yield a spatially continuous phase. The white line in the middle denotes the selected phase points for analysis. (c) Spatial phases along the white line in (b), for multiple different wavelengths, retrieved from seven different holograms. The camera pixel size is $3.5 \mu\text{m}$. The spatial phases show parabolic shapes with different tilts, indicating the presence of wave-front curvature and wave-front tilt dispersion.

Fig. 2(a). Note that we have not plotted the phase where the pulse intensity was near zero. To obtain a continuous phase envelope over space and time, we unwrapped the spatial phase using codes that aim to guarantee two-dimensional phase continuity and we plot the unwrapped phase in Fig. 3(b). Note that overall the phase has a parabolic shape along x and is nearly constant along y . The edges in the unwrapped phase still have minor 2π phase jumps. The tiny islands to the upper right of the phase plots were due to the reflection from the ANDF, which also appeared in the central hologram in Fig. 2(a).

To show that wave-front tilt dispersion was present, we must examine how these spatial phase-fronts changed with frequencies. We selected 155 points along the central row of the measured phase matrix, shown in Fig. 3(b) by a white line for the 800.05 nm phase. Then, at multiple different wavelengths [using seven holograms along the central row of Fig. 2(a)], we plotted the spatial phases along this white line, with respect to the position x . The resulting curves are shown in Fig. 3(c).

From Fig. 3(c), we see that each phase shows a parabolic shape over the horizontal position x . This means that, at all these wavelengths, the pulse showed wave-front curvature, meaning that the beam was diverging in the horizontal direction. A more interesting feature of these phase plots is that the peaks of the spatial phases shift from left to right over increasing wavelengths. Note again that these spatial phases each represent a wave-front for a certain wavelength, and the peak shift can be viewed as a superposition of parabolic phases with different linear phases tilted at different slopes. Therefore, the tilting difference of the wave-front over multiple wavelengths is the evidence of wave-front tilt dispersion in the pulse.

As stated before, because the spatiotemporal couplings in all Fourier domains are interrelated, the presence of both spatial chirp and wave-front tilt dispersion in the (x, ω) domain would indicate the presence of the ultrafast lighthouse effect in the spatial-frequency-temporal (k, t) domain. However, to more directly observe, we perform further analysis of the field below.

Equation (6) asserts that ultrafast lighthouse effect is present when pulse-front tilt and wave-front curvature are both present. Figure 3(c) already provides ample evidence on wave-front curvature at all wavelengths. If one can demonstrate that the measured pulse also has pulse-front tilt, then we must have the ultrafast lighthouse effect.

Pulse-front tilt is a difference in the pulse arrival time over a transverse spatial dimension. When pulse-front tilt is present, the retrieved spatio-spectral field $E(x, y, \omega)$ from STRIPED FISH will have different spectral-phase slopes at different positions across the beam. We therefore investigated the spectral phase at multiple different positions by analyzing a set of spatial points from the unwrapped phase. As in Fig. 4(a) [reproduced from Fig. 3(b)] for 800.05 nm, we selected five equally spaced points along the central row for their retrieved phases. We then plotted the spectral phases of these points as functions of angular frequency in Fig. 4(b). As expected, the resulting spectral phases showed very good linear dependences on angular frequency, which means that the pulse arrival time varied horizontally across the beam. We fit the linear spectral phases of each point, calculated the corresponding delays, and listed them on

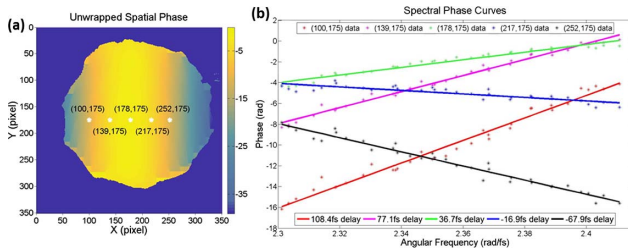


Fig. 4. Measured spectral phase by STRIPED FISH. (a) Spatial phase plot for 800.05 nm. Five points along the central row were selected to investigate the phase behavior over frequency. (b) Spectral phase curves at five different points as marked in (a). Spectral phase data were fit linearly over angular frequencies and the corresponding delays, which can be obtained from the slope of the curves, were listed at the bottom.

the bottom of the plot. Considering that the pulse had wave-front curvature from Fig. 3(c) and pulse-front tilt from Fig. 4(b), as discussed, it must possess the ultrafast lighthouse effect.

We can also observe the pulse-front tilt and ultrafast lighthouse effect by taking Fourier transforms of the retrieved electric field $E(x, y, t)$ and plotting the pulse intensity profiles with respect to time. We took the magnitude squares of the central row and column of the resulting spatiotemporal field $E(x, y, t)$, yielded the corresponding intensities $I(x, y, t)$ and $I(x, y, t)$, and plotted them in Figs. 5(a) and 5(c), respectively. Figure 5(a) shows that the pulse central-row intensity $I(x, y, t)$ had an arrival time depending linearly on x , which means that pulse-front tilt was present in the pulse. The ghost structures in plots of Fig. 5 were due to the frequency-domain interpolation and the limited space windows used for the Fourier transforms, and

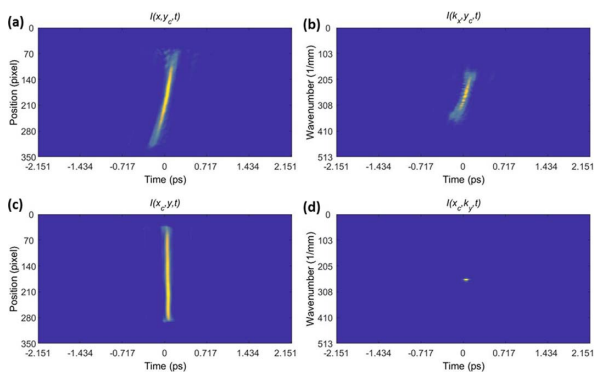


Fig. 5. Pulse intensities in the spatiotemporal (x, t) domain and spatial-frequency-temporal (k, t) domain. (a) Pulse intensity along the central row in the spatiotemporal domain. The intensity $I(x, y, t)$, with closely linear dependence between x and t , indicates the presence of pulse-front tilt. (b) Pulse intensity $I(k_x, y, t)$ along the central row after Fourier transforming $E(x, y, t)$ into the spatial-frequency-temporal domain. Linear dependence between k_x and t is an indication of ultrafast lighthouse effect. (c) Pulse intensity along the central column in the spatiotemporal domain. The field intensity $I(x, y, t)$ shows a span over y , and essentially no pulse-front tilt. (d) Pulse intensity $I(x, y, t)$ along the central column in the spatial-frequency-temporal domain, where it shows no coupling between k_y and t compared to (b).

the beam edges appeared more vulnerable to these effects. In all these plots, nevertheless, the pulse intensity behaviors were still very clear and pulses were much more prominent than the noisy structures. Along the y direction, as shown in Fig. 5(c), the arrival time of the central-column pulse intensity $I(x, y, t)$ showed less dependence on space and time, and therefore no obvious amplitude couplings between y and t and minimal pulse-front tilt in y , as intended.

A similar approach in the spatial-frequency-temporal (k, t) domain can show the presence of ultrafast lighthouse effect. We performed a one-dimensional Fourier transform on the central-row and central-column field slices $E(x, y, t)$ and $E(x, y, t)$ with respect to the spatial coordinates x and y , respectively, yielding the (k, t) domain fields $E(k_x, y, t)$ and $E(x, k_y, t)$. Then we plotted their intensities $I(k_x, y, t)$ and $I(x, k_y, t)$ in Figs. 5(b) and 5(d), respectively. Figure 5(b) shows that the horizontal slice $I(k_x, y, t)$ had a closely linear dependence on the spatial frequency k_x and time t , so the pulse propagation direction changed with time. In other words, this linear dependence between k_x and time t means the presence of the ultrafast lighthouse effect. For comparison, the vertical slice $I(x, k_y, t)$ showed essentially no pulse amplitude coupling between the spatial frequency k_y and time t .

Plotting the full pulse field, including its all intensity and phase variations over (x, y, z, t) or (x, y, z, ω) , is a quite complex task. This is true especially when the pulse contains spatial phase variations and when the field involves spatial-frequency (k) couplings. To address this issue and effectively plot the information obtained by STRIPED FISH, we developed a method to plot the pulse in 3D, where we use brightness for the intensity and colors for spectral energy distribution. Because the phase is responsible for the frequency distributions, using color distribution to represent phase is natural and meaningful [31]. To show the impact of spatial phase variations over the longitudinal dimension z , we calculated diffraction integrals to determine how the measured pulse evolved in space.

In Fig. 6, we show the propagation of the measured electric field and compare it to a simulated pulse. We set $z = 0$ at the focus. The STRIPED FISH measurement plane was at $z = 82$ mm, just outside the plotted range. The simulated beam was defined using the measured spectrum and the average spectral phase, which should be constant as the beam propagated in free space. Based on the experimental apparatus, the simulated pulse was given pulse-front tilt and wave-front curvature. By plotting the pulse at several z planes, we can display the longitudinal features of the measured field. We have achieved good agreement between the measured and simulated pulse propagations. Shown in Figs. 6(a) and 6(c), both the measured and the simulated pulses had a focusing behavior in the x - z plane, with spatial chirp and different tilting before and after the focus.

The ultrafast lighthouse effect can be illustrated by a movie in space and time, with snapshots shown in Figs. 6(b) and 6(d). The agreement of experimentally measured and simulated pulse movies (see Visualization 1 and Visualization 2) confirms our understanding and measurement of this effect. Spatial chirp and the lighthouse propagation can be very clearly shown by the movies. In the vertical direction, the pulse spatiotemporal

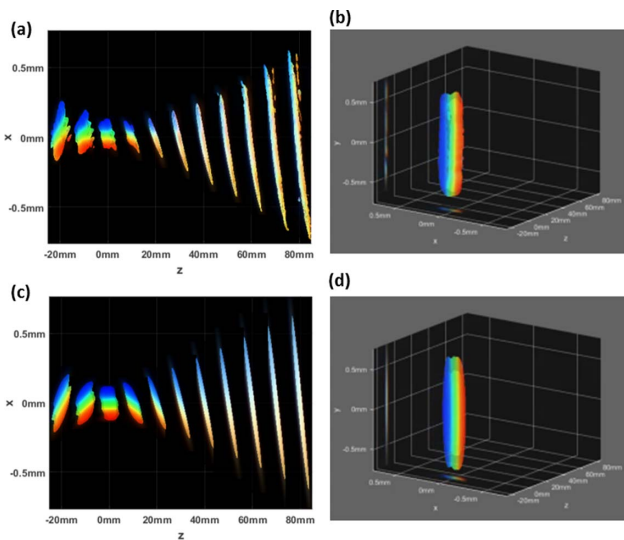


Fig. 6. Pulse propagation plots and movies of the ultrafast lighthouse effect. The longitudinal propagation behavior was determined by calculating diffraction integrals. (a) Overhead view of the measured pulse evolution in the x - z plane. The pulse focusing, spatial chirp, and ultrafast lighthouse effect were clearly shown. (b) Movie snapshot of pulse propagation in the x - y - z space. The movie (see Visualization 1) provides a perspective view and also sidewall projections of the measured pulse. (c) Overhead view of the simulated pulse. (d) Movie snapshot of the simulated pulse (see Visualization 2).

behaviors were relatively simpler, as can be observed from the pulse itself and also projections on the side walls of the movie. In the retrieved pulse animation, the spatial resolution is reflected by the camera pixel size of $3.5 \mu\text{m}$. The time resolution was based on the spectral range of the measurement, which corresponds to a temporal resolution of 57 fs. The animation has a finer temporal sampling in each frame, which was interpolated based on the measured data. The spectral resolution was 3–5 nm per each hologram, determined by the filter bandwidth. The measured bandwidth was about 40 nm and the limit of measured bandwidth would be about 50 nm, which can potentially be extended by using DOE that gives more divergent beams and tighter focusing imaging optics.

5. CONCLUSIONS

Using the complete spatiotemporal pulse measurement technique STRIPED FISH, we measured the ultrafast lighthouse effect in femtosecond laser pulses. The ultrafast lighthouse effect was generated by focusing a pulse with pulse-front tilt, implemented by a pair of prisms and a cylindrical focusing lens. Using the STRIPED FISH trace and the retrieved results, we discussed the presence of ultrafast lighthouse effect and its relationship to other spatiotemporal couplings. By transforming the measured field into spatial-frequency-temporal (k, t) domain, we directly observed a pulse amplitude coupling with near-linear dependence, i.e., the ultrafast lighthouse effect. To demonstrate the lighthouse, we developed a 3D movie-plotting approach to include both transverse and longitudinal field variations, giving an intuitive view of the pulse propagation over space and time. Finally, we should point out that

STRIPED FISH measurement is quite general and makes no assumptions about the pulse waveform or the spatiotemporal couplings, so this technique can potentially measure arbitrary couplings or distortions and is an ideal method for measuring various possible distortions in pulses over space and time.

Funding. National Science Foundation (NSF) (ECCS-1307817); Georgia Research Alliance (GRA).

Acknowledgment. Rick Trebino owns a company that sells pulse-measurement devices.

REFERENCES

1. A. M. Weiner, J. P. Heritage, and E. Kirschner, "High-resolution femtosecond pulse shaping," *J. Opt. Soc. Am. B* **5**, 1563–1572 (1988).
2. O. Katz, E. Small, Y. Bromberg, and Y. Silberberg, "Focusing and compression of ultrashort pulses through scattering media," *Nat. Photonics* **5**, 372–377 (2011).
3. G. Zhu, J. Van Howe, M. Durst, W. Zipfel, and C. Xu, "Simultaneous spatial and temporal focusing of femtosecond pulses," *Opt. Express* **13**, 2153–2159 (2005).
4. C. Fiorini, C. Sauteret, C. Rouyer, N. Blanchot, S. Seznec, and A. Migus, "Temporal aberrations due to misalignments of a stretcher-compressor system and compensation," *IEEE J. Quantum Electron.* **30**, 1662–1670 (1994).
5. Z. Bor, "Distortion of femtosecond laser pulses in lenses and lens systems," *J. Mod. Opt.* **35**, 1907–1918 (1988).
6. H. Kumagai, S.-H. Cho, K. Ishikawa, K. Midorikawa, M. Fujimoto, S.-I. Aoshima, and Y. Tsuchiya, "Observation of the complex propagation of a femtosecond laser pulse in a dispersive transparent bulk material," *J. Opt. Soc. Am. B* **20**, 597–602 (2003).
7. D. E. Adams, T. A. Planchon, A. Hrin, J. A. Squier, and C. G. Durfee, "Characterization of coupled nonlinear spatio-spectral phase following an ultrafast self-focusing interaction," *Opt. Lett.* **34**, 1294–1296 (2009).
8. Z. Bor, B. Racz, G. Szabo, M. Hilbert, and H. Hazim, "Femtosecond pulse front tilt caused by angular dispersion," *Opt. Eng.* **32**, 2501–2504 (1993).
9. J. Hebling, "Derivation of the pulse front tilt caused by angular dispersion," *Opt. Quantum Electron.* **28**, 1759–1763 (1996).
10. P. Bowlan and R. Trebino, "Extreme pulse-front tilt from an etalon," *J. Opt. Soc. Am. B* **27**, 2322–2327 (2010).
11. S. Akturk, X. Gu, E. Zeek, and R. Trebino, "Pulse-front tilt caused by spatial and temporal chirp," *Opt. Express* **12**, 4399–4410 (2004).
12. S. Akturk, X. Gu, P. Gabolde, and R. Trebino, "The general theory of first-order spatio-temporal distortions of Gaussian pulses and beams," *Opt. Express* **13**, 8642–8661 (2005).
13. S. Akturk, X. Gu, P. Bowlan, and R. Trebino, "Spatio-temporal couplings in ultrashort laser pulses," *J. Opt.* **12**, 093001 (2010).
14. A. Kostenbauder, "Ray-pulse matrices: a rational treatment for dispersive optical systems," *IEEE J. Quantum Electron.* **26**, 1148–1157 (1990).
15. V. Chauhan, P. Bowlan, J. Cohen, and R. Trebino, "Single-diffraction-grating and grism pulse compressors," *J. Opt. Soc. Am. B* **27**, 619–624 (2010).
16. A. M. Weiner, "Femtosecond pulse shaping using spatial light modulators," *Rev. Sci. Instrum.* **71**, 1929–1960 (2000).
17. E. Block, J. Thomas, C. Durfee, and J. Squier, "Integrated single grating compressor for variable pulse front tilt in simultaneously spatially and temporally focused systems," *Opt. Lett.* **39**, 6915–6918 (2014).
18. D. Asoubar, R. Kammel, S. Nolte, and F. Wyrowski, "Analysis of pulse front tilt in simultaneous spatial and temporal focusing," *J. Opt. Soc. Am. A* **31**, 591–2446 (2014).
19. R. Wyatt and E. E. Marinero, "Versatile single-shot background-free pulse duration measurement technique for pulses of subnanosecond to picosecond duration," *Appl. Phys.* **25**, 297–301 (1981).

20. T. C. Wong and R. Trebino, "Single-frame measurement of complex laser pulses tens of picoseconds long using pulse-front tilt in cross-correlation frequency-resolved optical gating," *J. Opt. Soc. Am. B* **30**, 2781–2786 (2013).
21. P. Bowlan and R. Trebino, "Complete single-shot measurement of arbitrary nanosecond laser pulses in time," *Opt. Express* **19**, 1367–1377 (2011).
22. S. Akturk, M. Kimmel, P. O'Shea, and R. Trebino, "Measuring pulse-front tilt in ultrashort pulses using GRENOUILLE," *Opt. Express* **11**, 491–501 (2003).
23. J. A. Wheeler, A. Borot, S. Monchocé, H. Vincenti, A. Ricci, A. Malvache, R. Lopez-Martens, and F. Quéré, "Attosecond lighthouses from plasma mirrors," *Nat. Photonics* **6**, 829–833 (2012).
24. K. T. Kim, C. Zhang, T. Ruchon, J.-F. Hergott, T. Auguste, D. Villeneuve, P. Corkum, and F. Quéré, "Photonic streaking of attosecond pulse trains," *Nat. Photonics* **7**, 651–656 (2013).
25. T. Hammond, K. T. Kim, C. Zhang, D. Villeneuve, and P. Corkum, "Controlling attosecond angular streaking with second harmonic radiation," *Opt. Lett.* **40**, 1768–1770 (2015).
26. C. Zhang, G. Vampa, D. Villeneuve, and P. Corkum, "Attosecond lighthouse driven by sub-two-cycle, 1.8 μm laser pulses," *J. Phys. B* **48**, 061001 (2015).
27. H. Vincenti and F. Quéré, "Attosecond lighthouses: how to use spatiotemporally coupled light fields to generate isolated attosecond pulses," *Phys. Rev. Lett.* **108**, 113904 (2012).
28. T. Auguste, O. Gobert, T. Ruchon, and F. Quéré, "Attosecond lighthouses in gases: a theoretical and numerical study," *Phys. Rev. A* **93**, 033825 (2016).
29. T. Hammond, G. G. Brown, K. T. Kim, D. Villeneuve, and P. Corkum, "Attosecond pulses measured from the attosecond lighthouse," *Nat. Photonics* **10**, 171–175 (2016).
30. P. Gabolde and R. Trebino, "Single-shot measurement of the full spatiotemporal field of ultrashort pulses with multispectral digital holography," *Opt. Express* **14**, 11460–11467 (2006).
31. Z. Guang, M. Rhodes, M. Davis, and R. Trebino, "Complete characterization of a spatiotemporally complex pulse by an improved single-frame pulse-measurement technique," *J. Opt. Soc. Am. B* **31**, 2736–2743 (2014).
32. R. Trebino, K. W. DeLong, D. N. Fittinghoff, J. N. Sweetser, M. A. Krumbügel, and D. J. Kane, "Measuring ultrashort laser pulses in the time-frequency domain using frequency-resolved optical gating," *Rev. Sci. Instrum.* **68**, 3277–3295 (1997).
33. R. Trebino, *Frequency-Resolved Optical Gating: The Measurement of Ultrashort Laser Pulses* (Kluwer, 2002).
34. Z. Guang, M. Rhodes, and R. Trebino, "Numerical simulations of holographic spatio-spectral traces of spatiotemporally distorted ultrashort laser pulses," *Appl. Opt.* **54**, 6640–6651 (2015).
35. H. Vincenti, A. Borot, T. Hammond, K. T. Kim, J. Wheeler, C. Zhang, T. Ruchon, T. Auguste, J. Hergott, and D. Villeneuve, "Applications of ultrafast wavefront rotation in highly nonlinear optics," *J. Phys. B* **47**, 124004 (2014).
36. P. O'Shea, M. Kimmel, X. Gu, and R. Trebino, "Highly simplified device for ultrashort-pulse measurement," *Opt. Lett.* **26**, 932–934 (2001).